AD-A031 336 NAVAL UNDERWATER SYSTEMS CENTER NEW LONDON CONN NEW --ETC F/G 17/1
PERFORMANCE ANALYSIS OF A SPLIT-BEAM AUTOMATIC TARGET FOLLOWER --ETC(U
SEP 76 W K FISCHER

UNCLASSIFIED NUSC-TR-5307 NL

1 OF 1
ADA031336

END

DATE FILMED
12 - 76

(12) 1-J

Performance Analysis of a Split-Beam Automatic Target Follower in Adverse Acoustic Environments

Wolfgang K. Fischer
Special Projects Department

9 September 1976

NUSC

NAVAL UNDERWATER SYSTEMS CENTER
Newport, Rhode Island • New London, Connecticut

PREFACE

This research was conducted under NUSC Project No. A-126-01, "Low SNR Processing," Principal Investigator, C. D. Mason (Code 325), and under Program Element 6000N, Subproject No. SS0122, Program Manager, W. J. Bundy (NISC, Code 2252).

The Technical Reviewer for this report was Dr. A. VanWoerkom (Code 101).

E. B. Siborg (Code 3211) was responsible for the computer programming results presented in this report. This work and his critical questioning are greatly appreciated.

REVIEWED AND APPROVED: 9 September 1976

W. A. Von Winkle
Head, Special Projects Department

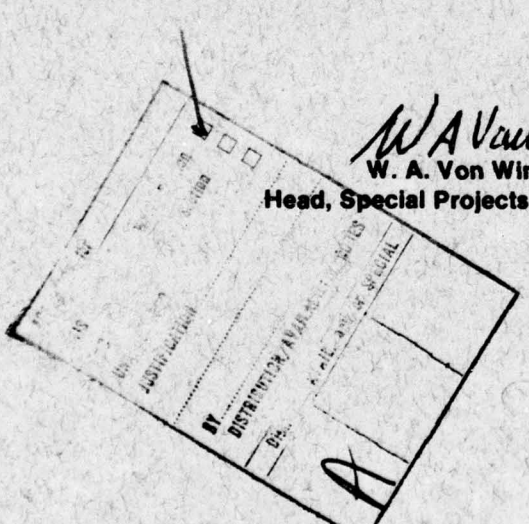

The author of this report is located at the New London Laboratory, Naval Underwater Systems Center, New London, Connecticut 06320.

UNCLASSIFIED

SECURITY CLASSIFICATION OF THIS PAGE (When Data Entered)

REPORT DOCUMENTATION PAGE

READ INSTRUCTIONS BEFORE COMPLETING FORM

1. REPORT NUMBER: TR 5307

2. GOVT ACCESSION NO.

3. RECIPIENT'S CATALOG NUMBER

4. TITLE (and Subtitle): PERFORMANCE ANALYSIS OF A SPLIT-BEAM AUTOMATIC TARGET FOLLOWER IN ADVERSE ACOUSTIC ENVIRONMENTS.

5. TYPE OF REPORT & PERIOD COVERED: Technical Rept.

6. PERFORMING ORG. REPORT NUMBER

7. AUTHOR(s): Wolfgang K. Fischer

8. CONTRACT OR GRANT NUMBER(s)

9. PERFORMING ORGANIZATION NAME AND ADDRESS
Naval Underwater Systems Center
New London Laboratory
New London, CT 06320

10. PROGRAM ELEMENT, PROJECT, TASK AREA & WORK UNIT NUMBERS
A-126-01

52p.

11. CONTROLLING OFFICE NAME AND ADDRESS
Naval Intelligence Support Center (NISC)
Washington, DC 20390

12. REPORT DATE
9 Sep[illegible]976

13. NUMBER OF PAGES
50

14. MONITORING AGENCY NAME & ADDRESS(if different from Controlling Office)
NUSC-TR-5307

15. SECURITY CLASS. (of this report)
UNCLASSIFIED

15a. DECLASSIFICATION/DOWNGRADING SCHEDULE

16. DISTRIBUTION STATEMENT (of this Report)

Approved for public release; distribution unlimited.

17. DISTRIBUTION STATEMENT (of the abstract entered in Block 20, if different from Report)

NUSC-A-126-01, SS-0122

18. SUPPLEMENTARY NOTES

19. KEY WORDS (Continue on reverse side if necessary and identify by block number)

Adverse Acoustic Environments
Automatic Target Follower (ATF)
Bearing Deviation Indicator (BDI)
Closed-Loop Analysis
Steady-State Bias Error
Steady-State Random Errors
Transcendental Equations

20. ABSTRACT (Continue on reverse side if necessary and identify by block number)

Steady-state bias and random errors are derived for an analog automatic target follower (ATF) whose inputs are sample functions of a stationary zero mean Gaussian random process. The result is in the form of two coupled transcendental equations that include the effects of correlated noise, interfering targets, and multipath. Specific values of the bias and random errors require the simultaneous solution of these two equations for any given set of acoustic conditions. Several examples are cited to

DD FORM 1 JAN 73 1473 EDITION OF 1 NOV 65 IS OBSOLETE
S/N 0102-014-6601

UNCLASSIFIED
SECURITY CLASSIFICATION OF THIS PAGE (When Data Entered)

405 918

20. (Cont'd)

illustrate the performance and threshold characteristics of a typical ATF operating in adverse acoustic environments.

TABLE OF CONTENTS

LIST OF ILLUSTRATIONS

PERFORMANCE ANALYSIS OF A SPLIT-BEAM AUTOMATIC TARGET FOLLOWER IN ADVERSE ACOUSTIC ENVIRONMENTS

INTRODUCTION

Present performance analyses of broadband split-beam bearing trackers can be grouped into two categories:

1. the open-loop analysis of trackers searching for a stationary target in a relatively general noise field[1-4] and

2. the closed-loop analysis of trackers searching for a dynamic target in a simple, specific noise field.[5-7]

The results of reports referenced under category 1 generally yield performance bounds, that is, values of bias and random errors under a specific set of acoustic conditions that can only be approached by any practical automatic target follower (ATF).

On the other hand, those referenced under category 2 yield design criteria on the feedback loop. By linearizing the bearing deviation indicator (BDI) about the expected operating point and using conventional control theory, a conceptually simple model is obtained for a very complex control problem. Unfortunately, the model is strictly applicable only to a single moving target in an uncorrelated ambient noise background.

In contrast, this report presents a closed-loop analysis of an ATF that is searching for one or more stationary targets in a relatively general noise field. The analytical technique differs from that of category 2 in one important respect. Whereas the controlled delay (ε) in the BDI shown in figure 1 is initially (before linearization) assumed to be deterministic, ε is considered to be a random variable in this report.

As a result of this more general approach, two coupled, transcendental equations involving the mean and variance of ε are obtained. A simultaneous graphic solution of these equations will then yield specific values of the bias and random errors for any given adverse acoustic environment.

In order to focus on the ATF analysis, only a two-element array is postulated. However, the derivation described in appendix A may readily be modified to include any array geometry.

DISCUSSION--BDI WITH RANDOM TIME DELAY

The BDI considered in this report is the analog anticorrelator shown in figure 1, where the inputs $w_1(t)$ and $w_2(t)$ are assumed to be sample functions of a stationary zero mean Gaussian random process. Filters h(t) and y(t) are real; additionally, y(t) must be odd* so that the device is, in fact, a deviation indicator. As indicated in figure 1, a 90^0 phase shifter or a differentiator satisfies this latter requirement. Finally, the random time delay (ε) is assumed to be uncorrelated from $w_1(t)$ and $w_2(t)$.

In appendix A, the mean (m_u) and the variance (σ_u^2) of the BDI output u are derived in terms of the characteristic function of an arbitrary random time delay (ε). It is further shown that if ε is Gaussian with mean m and variance σ^2, then

$$m_u(m,\sigma^2) = \int df\ \phi_{12}(f) e^{i2\pi fm}\ e^{-1/2(2\pi f\sigma)^2} \tag{1}$$

$$\sigma_u{}^2(m,\sigma^2) = \sum_{n=1,2,\ldots}^{\infty} \frac{\sigma^{2n}}{n!} \left(\frac{\partial^n m_u}{\partial m^n}\right)^2 + \int G_{NN}(f,m,\sigma^2)df, \tag{2}$$

where

$$G_{NN}(f,m,\sigma^2) = \phi_1(f) \circledast \phi_2(f) + \int dx\ \phi_{12}(x)\ \phi_{12}(x - f) e^{i2\pi m(2x - f)} \cdot e^{-1/2[2\pi s(2x - f)]^2}, \tag{3}$$

*Alternatively, the requirement on y(t) is that its transform (Y(f)) must be purely imaginary and odd. $Y(f) = Y^*(-f) = -Y(-f)$.

$$\phi_1(f) = |H(f)|^2 \, G_{w_1 w_1}(f) \qquad m = \bar{\varepsilon}$$

$$\phi_2(f) = |H(f)|^2 \, |Y(f)|^2 \, G_{w_2 w_2}(f) \qquad \sigma^2 = \overline{\varepsilon^2} - \bar{\varepsilon}^2$$

$$\phi_{12}(f) = |H(f)|^2 \, Y^*(f) \, G_{w_1 w_2}(f),$$

where

$\circledast$ = denotes convolution,

$G_{w_1 w_1}(f)$ = auto-spectral density of input $w_1(t)$,

$G_{w_2 w_2}(f)$ = auto-spectral density of input $w_2(t)$,

$G_{w_1 w_2}(f)$ = cross-spectral density of inputs $w_1(t)$ and $w_2(t)$, and

$H(f)$ and $Y(f)$ = Fourier transforms of filter $h(t)$ and $y(t)$, respectively.

As noted in appendix A, $G_{NN}(f)$ represents the average (averaged over ε) auto-spectral density of a random variable (N), which, at a given ε, is the deviation of u from its mean ($\bar{u}$). It is a generalized form of the equivalent noise source or disturbing perturbation used by Lindgren[6] and others to account for the finite averaging time of the closed-loop filter.

In order to appreciate the effect of the randomness of ε on the output (u), consider the mean and variance of u when the "jitter" is zero, that is, when ε is deterministic with value m and $\sigma = 0$. Under this condition,

$$m_u = \int df \, \phi_{12}(f) \, e^{i2\pi fm} \tag{4}$$

$$\sigma_u^2 = \int df \left[\phi_1(f) \circledast \phi_2(f) + \phi_{12}(f) \, e^{i2\pi fm} \circledast \phi_{12}^*(f) e^{-i2\pi fm} \right]. \tag{5}$$

Notice that the infinite series in equation (2) vanishes when $\sigma = 0$. The reader may confirm that these are the usual expressions found in the literature for the analog BDI shown in figure 1.

As the jitter increases ($\sigma \neq 0$), m_u will decrease from its maximum value given in equation (4), whereas σ_u^2 will generally increase because the contribution from the infinite series in equation (2) is greater than the decrease in $G_{NN}(f)$ (see equation 3). Finally, as the jitter becomes very large, m_u approaches zero for all inputs; however, σ_u^2 approaches some limiting value. The interpretation of this behavior is that the output signal-to-noise ratio (SNR) approaches zero.

ATF ANALYSIS

The complete ATF is formed by "feeding" the BDI output (u(t)) into an appropriate feedback filter (z(t)) and using its output (v(t)) to control the delay ($\varepsilon(t)$). Figure 2 shows the resultant circuit to be analyzed. The dashed line represents that portion of the feedback loop that will be closed in the following discussion.

It is assumed in this analysis that the effective integration time of the closed loop is much longer than the correlation time of the inputs. Thereby, when the loop is closed, v(t) approaches a similar (but not the same) Gaussian distribution as that assumed for ε in the derivation of equations (1) and (2).

STEADY-STATE MEAN CALCULATION

If we assume that the loop is open, the expectation (m_v) of the random variable (v) is given by

$$m_v = Z(0)m_u, \tag{6}$$

where Z(0) is the dc gain of the feedback filter whose units are such that v has units of time (sec).

The loop is now closed in the usual manner by stipulating that, in the steady state, the mean of ε be equal to the mean of v. Using equation (1) and denoting the steady-state values of m and σ as m_o and σ_o, respectively, yields

$$m_o = m_v = Z(0)m_u = Z(0)\int df\ \phi_{12}(f)e^{i2\pi f m_o}e^{-1/2(2\pi f\sigma_o)^2}, \qquad (7)$$

which is a transcendental equation in m_o whose solutions represent possible steady-state values of m for any given value of σ_o^2.

Typically, the feedback filter (Z(f)) is at least of the first order, so that Z(0) tends to infinity. Equation (7) then reduces to

$$m_u = \int df\ \phi_{12}(f)e^{i2\pi f m_o}\ e^{-1/2(2\pi f\sigma_o)^2} = 0. \qquad (8)$$

Thus, for a given σ_o, the possible steady-state values of m are given by those values for which the mean BDI output (error function) is zero, e.g., by the zero crossing of the error function.

Notice that the derivation of equation (7) or (8) has not required any linearization. Furthermore, these expressions are valid for any stationary inputs ($w_1(t)$ and $w_2(t)$) provided the effective integration time of the loop filter is large with respect to the correlation time of the inputs.

STEADY-STATE RANDOM ERROR CALCULATION

The small steady-state random deviations of ε may be obtained by the usual practice of linearizing the BDI and using control theory to derive the closed-loop transfer function. For this purpose, assume that the ATF has achieved a steady-state condition, so that the fluctuations in the BDI output are only due to the jitter of ε. Denoting the steady-state values of m and σ by m_o and σ_o, respectively, we see in appendix B that the variance of the BDI output about this operating point is given approximately by

$$\sigma_u^2(m_o,\sigma^2) \cong \sigma^2 K_{BDI}^2(m_o,\sigma_o^2) + \int G_{NN}(f,m_o,\sigma_o^2)df, \qquad (9)$$

where

$$K_{BDI}^2(m_o\sigma_o^2) \equiv \left(\frac{\partial m_u}{\partial m}\right)^2_{\substack{m = m_o \\ \sigma = \sigma_o}} + \left(\frac{\partial m_u}{\partial \sigma}\right)^2_{\substack{m = m_o \\ \sigma = \sigma_o}}. \qquad (10)$$

Now, in the steady state, the mean of the BDI output is zero and its variance is given by equation (9). A linear system that matches these requirements is shown in figure 3 if the mean of the equivalent noise source (N') is zero and if its spectral density is $G_{NN}(f, m, \sigma^2)$.

By convention, $K_{BDI}(m_o,\sigma_o^2)$ is denoted as the "BDI gain." With reference to equation (10), the gain is equal to the <u>total</u> derivative (variation) of the error function and, therefore, represents a more general form of the conventional BDI gain expression. Further comparison shows that when σ_o is small, the first term in (10) dominates, and K_{BDI} reduces (for zero bias error) to the expression obtained by Pinkos[7] and Develet.[8]

It should be noted that the linearized model of the BDI, as shown in figure 3, is applicable only at the steady-state operating point, and its usefulness is limited to determining the steady-state jitter (σ_o).

Accordingly, after passing the BDI output (u) through the feedback filter (z), the ATF loop may be closed, as shown in figure 4(a). Via conventional control theory, the equivalent closed-loop filter (A(f)), which relates the input (N'(t)) to the output ($\varepsilon(t)$), is given by

$$A(f) = \frac{Z(f)}{1 + K_{BDI}\, Z(f)} . \tag{11}$$

Finally, with reference to figure 4(b), and remembering that $\overline{N'} = 0$, the variance of ε becomes

$$\sigma_o^2 = \int df\; G_{N'N'(f)}\; |A(f)|^2 = \int df\; G_{NN}(f)\; \left|\frac{Z(f)}{1 + K_{BDI} Z(f)}\right|^2 \tag{12}$$

Under the initial assumption of long integration times, the bandwidth of $|A|^2$ will be much smaller than that of $G_{N'N'}$, so that, to a good approximation, the variance is given by

$$\sigma_o^2 \cong \frac{G_{NN}(0,m_o,\sigma_o^2)}{\left|K_{BDI}(m_o,\sigma_o^2)\right|^2} \int df\; \left|\frac{K_{BDI}(m_o,\sigma_o^2)\; Z(f)}{1 + K_{BDI}(m_o,\sigma_o^2)\; Z(f)}\right|^2, \tag{13}$$

where, from equation (3),

$$G_{NN}(0,m_o,\sigma_o^2) = \int df \left[\phi_1(f)\,\phi_2(f) + \phi_{12}^2(f)\, e^{i4\pi f m_o}\, e^{-1/2(4\pi f\sigma_o)^2}\right]. \tag{14}$$

Substituting for ϕ_1, ϕ_2, ϕ_{12} and making use of the restrictions imposed on Y(f) yields

$$G_{NN}(0,m_o,\sigma_o^2) = \int df\, |H(f)|^4\, |Y(f)|^2 \left[G_{w_1w_1}(f)\, G_{w_2w_2}(f) - G_{w_1w_2}^2(f) e^{i4\pi f m_o}\, e^{-1/2(4\pi f\sigma_o)^2}\right]. \tag{15}$$

Typically, one defines the integral in equation (13) as the equivalent closed-loop bandwidth (Δf_e); that is,

$$\Delta f_e(m_o,\sigma_o^2) \equiv \int \left|\frac{K_{BDI}(m_o,\sigma_o^2)\, Z(f)}{1 + K_{BDI}(m_o,\sigma_o^2)\, Z(f)}\right|^2 df. \tag{16}$$

Thereby, equation (13) becomes

$$\sigma_o^2 \cong \frac{G_{NN}(0,m_o,\sigma_o^2)}{\left|K_{BDI}(m_o,\sigma_o^2)\right|^2}\ \Delta f_e(m_o,\sigma_o^2) \tag{17}$$

Notice that equation (17) is also a transcendental equation in σ_o whose solutions, for a given value of m_o, are possible steady-state values of the random error. Finally, the simultaneous solutions to equations (8) and (17) represent possible steady-state values for the mean and variance of the random time delay (ε). Such an analysis for a typical ATF and for four adverse acoustic environments is presented in the next section.

TYPICAL RESULTS

In this section, the steady-state bias and random errors are calculated for a typical ATF that is operating in four adverse acoustic environments:

Case I -- single target in uncorrelated noise
Case II -- single target in partially correlated noise
Case III -- single target in uncorrelated noise plus interference
Case IV -- single target with multipath in uncorrelated noise

In all these acoustic environments, the signal, noise, and interference spectral densities are assumed to be uniform; the noise power is assumed to be equal at each input; and the direct-path signal spectral density is assumed to be unity.

With reference to figure 5, the general ATF inputs $w_1(t)$ and $w_2(t)$ for the four environments are

$$w_1(t) = S(t + t_{OS1}) + \beta S(t + t_{OS2}) + I(t + t_{OI}) + n_1(t)$$

$$w_2(t) = S(t + t_{OS1} + t_{S1}) + \beta S(t + t_{OS2} + t_{S2}) + I(t + t_{OI} + t_I) + n_2(t), \quad (18)$$

where

S = desired signal (direct path)

βS = multipath signal

I = interfering signal

n_1, n_2 = noise

t_{OS1} = bulk time delay of the direct signal

t_{OS2} = bulk time delay of the multipath signal

t_{OI} = bulk time delay of the interfering signal

$t_{S1} = \frac{d}{C} \sin\theta_{S1}$ - interelement delay of the direct signal

$t_{S2} = \frac{d}{C} \sin\theta_{S2}$ - interelement delay of the multipath signal

$t_I = \frac{d}{C} \sin\theta_I$ - interelement delay of the interfering signal

d = sensor spacing

C = speed of sound in water

θ_{S1} = arrival angle of the direct signal with respect to broadside

θ_{S2} = arrival angle of the multipath signal with respect to broadside

θ_I = arrival angle of the interfering signal with respect to broadside

β = amplitude ratio of the multipath signal with respect to the direct signal

Accordingly, the auto- and cross-spectral densities of $w_1(t)$ and $w_2(t)$ are

$$G_{w_1w_2}(f) = 1 + \beta^2 + 2\beta \cos 2\pi f t_o + G_{II} + G_{nn} \tag{19}$$

$$G_{w_2w_2}(f) = 1 + \beta^2 + 2\beta \cos 2\pi f(t_o + t_{S1} - t_{S2}) + G_{II} + G_{nn} \tag{20}$$

$$G_{w_1w_2}(f) = e^{-i2\pi f t_{S1}} + \beta e^{-i2\pi f(t_{S2} - t_o)} + \beta e^{-i2\pi f(t_{S1} + t_o)}$$

$$+ \beta^2 e^{-i2\pi f t_{S2}} + G_{II}\, e^{-i2\pi f t_I} + \gamma(f) G_{nn} \tag{21}$$

where the previous assumptions regarding the acoustic fields have been incorporated and where

$$t_0 = t_{0S1} - t_{0S2}$$

$$\gamma(f) = \gamma_{n_1 n_2}(f) \equiv \frac{G_{n_1 n_2}(f)}{G_{nn}} = \text{noise coherence.}$$

Notice that for the above assumptions, G_{II} and G_{nn} may be interpreted as the interference-to-signal and noise-to-signal ratio, respectively.

The particular ATF configuration considered for these four acoustic environment cases is shown in figure 6. Additional particulars are as follows:

$$|H(f)|^2 = \begin{cases} 1 & 402.65 < |f| < 805.3 \\ 0 & \text{otherwise} \end{cases}$$

$$Y(f) = i2\pi f \text{ (differentiator)}$$

$$Z(f) = \frac{\alpha(1 + i2\pi fT/3)\ (1 + i2\pi fT/18)}{(i2\pi f)\ (1 + i2\pi fT)\ (1 + i2\pi fT/9)\ (1 + i2\pi fT/90)},$$

where $T = 50$ sec and α is a proportionality constant having units of sec/volt^2 whose value must be chosen in accordance with dynamic following considerations.

Substituting $Z(f)$ into equation (16) and performing the integration yields

$$\Delta fe = \frac{(\alpha K_{BDI} T)}{2T} \left[\frac{1 + 0.11(\alpha K_{BDI} T) + 0.001(\alpha K_{BDI} T)^2}{1 + 0.30(\alpha K_{BDI} T) + 0.0067(\alpha K_{BDI} T)^2}\right], \quad (22)$$

which, to a good approximation, is

$$\Delta fe \approx \frac{(\alpha K_{BDI} T)^{0.7}}{2T} \quad \text{for} \quad 1 < (\alpha K_{BDI} T) < 1000. \quad (23)$$

The restriction on α and, therefore, on the closed-loop bandwidth is determined by the maximum tolerable "lag distance." With reference to equation (16), the velocity error constant (K_v) is defined as

$$K_v \equiv \lim_{f \to 0} (i2\pi f) K_{BDI} Z(f) = K_{BDI} \alpha \ . \tag{24}$$

As shown in a Raytheon study,[5] a maximum allowable lag distance of 100 yd (91.44m) for a target that is moving at a constant speed of 40 knots requires that $K_v \geq 0.225$. Therefore, the value of α must be chosen so that, within the operating range of the ATF,

$$\alpha \geq \frac{0.225}{K_{BDI}} \quad \text{or} \quad (\alpha K_{BDI} T) > 11.25. \tag{25}$$

In order to demonstrate the procedure required to calibrate the ATF (chose α) and to solve for the steady-state values of m and σ, case I will be worked in detail. For the other examples, only the final results will be presented.

CASE I--SINGLE TARGET IN UNCORRELATED NOISE

The conditions for case I are

$$\beta = 0, \ I = 0, \ \gamma = 0,$$

so that equations (19)-(21) reduce to

$$G_{w_1 w_1}(f) = G_{w_2 w_2}(f) = 1 + G_{nn} \tag{26}$$

$$G_{w_1 w_2}(f) = e^{-i2\pi f t_{S1}} \tag{27}$$

Substituting equation (27) and the expressions for Y(f) and $|H(f)|^2$ into equation (8) yields

$$m_u = \frac{1}{\pi} \int_{\omega_1}^{\omega_2} \omega \sin \left[\omega(m_o - t_{S1})\right] \ e^{-1/2(\omega\sigma_o)^2} \ d\omega = 0, \tag{28}$$

where

$$\omega = 2\pi f,\ \omega_1 = 2\pi(402.65)\ \text{rad/sec},\ \omega_2 = 2\pi(805.3)\ \text{rad/sec}.$$

The error function (m_u) is plotted in figure 7 as a function of the bias error ($b = m_o - t_{S1}$) for zero jitter and for $\sigma_o = 0.25$ msec. In accordance with equation (28), possible solutions for b are given by the zero-crossings of this function. The locus of these solutions (zero-crossings) are shown as dotted lines in figure 8. It will be demonstrated shortly that some of these solutions are unstable while others cannot exist in the physical ATF due to the incorrect sign of the error function.

The gain of the BDI is obtained from equation (10) and the left side of equation (28):

$$K_{BDI} = \left\{ \left[\frac{1}{\pi} \int_{\omega_1}^{\omega_2} \omega^2 e^{-1/2(\omega\sigma_o)^2} \cos \omega(m_o - t_{S1}) d\omega \right]^2 + \left[\frac{\sigma_o}{\pi} \int_{\omega_1}^{\omega_2} \omega^3 e^{-1/2(\omega\sigma_o)^2} \sin \omega(m_o - t_{S1}) d\omega \right]^2 \right\}^{1/2}, \tag{29}$$

which is plotted in figures 9 and 10 as a function of bias error and random error, respectively.

Notice in figure 9 that, for fixed jitter, the gain of the BDI cycles with the bias error, with maxima occurring in the vicinity of the zero-crossings of the error function. Also, notice that the highest gain is always obtained at zero bias error.

The important feature to be observed in figure 10 is that, for small fixed bias errors, the BDI gain curves seem to "invert" about the point (T). That is, for $\sigma_o \leq 0.25$ msec, the gain decreases as b

increases; whereas, for $\sigma_o > 0.25$ msec, the gain increases as b increases. The significance of this phenomenon will become apparent shortly.

For the purpose of discussing system stability, it becomes expedient to use the approximate expression (23) for Δf_e. Substituting this into equation (17) and rearranging terms yields

$$\sigma_o^2 \; K_{BDI}^{1.3}(m_o,\sigma_o^2) = G_{NN}(0,m_o,\pi_o^2) \; \frac{(\alpha T)^{0.7}}{2T} \quad . \tag{30}$$

Also, substituting equation (26) and the expression for Y(f) and $|H(f)|^2$ into equation (15) yields

$$G_{NN}(0,m_o,\sigma_o^2) = \frac{1}{\pi} \int_{\omega_1}^{\omega_2} d\omega \;\; \omega^2 \left[(1 + G_{nn})^2 \right.$$

$$\left. - e^{-1/2(2\omega\sigma_o)^2} \cos 2\omega(m_o - t_{S1}) \right] . \tag{31}$$

For low SNR's, the auto-spectral density will become independent of m_o and σ_o, leaving

$$G_{NN}(0,m_o,\sigma_o^2) \approx \frac{7\omega_2^3 G_{nn}^2}{24\pi} \quad \text{for } G_{nn} >> 1. \tag{32}$$

Hence, for low SNR, the right side of equation (30) will be a constant (horizontal line) proportional to G_{nn}^2.

The graphic solution to equation (30) is shown in figure 11, where the left side of equation (30) is represented by solid curves and the right side of (30) is indicated, for some arbitrary G_{nn} and α, by the

dashed horizontal line. In accordance with (30), the intersections of the horizontal line with the solid curves represent possible steady-state solutions for σ. As the SNR decreases, the horizontal line will shift upward and the new intersections represent possible solutions at the higher noise level.

The question of system instability may be answered by proper interpretation of figure 11. Consider the operating point at Q_1(σ = 0.2 msec, b = 0.15 msec). Suppose that the SNR is fixed and that there occurs an incremental increase in b. The new operating point will be located on the horizontal line and to the right of Q_1; that is, an incremental increase in the bias results in a operating point Q_1' whose jitter is higher than that of Q_1. Similar considerations at operating point Q_2 cause a shift to the left; that is, at Q_2 an increase in bias yields a decrease in jitter. Clearly, Q_2 is an unstable operating point. One may, therefore, establish the following stability criterion:

1. An operating point is considered to be stable if, at a fixed SNR, an increase in b yields an increase in σ.

2. An operating point is considered to be unstable if, at a fixed SNR, an increase in b yields a decrease in σ.

An operating point where an incremental increase in the bias error results in no change in σ represents a point on the threshold of stability/instability. Point T, discussed in connection with figure 10 and also indicated in figure 11, is one such operating point. In general, the coordinates of the threshold operating points are given by the location of the extremes (maxima and minima) of figure 9.

Figure 8 shows the locus of these threshold operating points (solid curves), as well as the locus of the zero-crossings of the error function (dashed curves). The shaded regions of this figure represent unstable operating regions, in accordance with the previously defined stability criterion. Also, figure 8 shows four possible stable operating modes of the ATF for a single target in uncorrelated noise at low SNR's. From figure 7, two of these modes (at b $\approx$ 0.8 msec and b $\approx$ 2.25 msec) may be discounted since the sign of the error function is such as to drive the operating point away from these zero-crossings. Alternatively, one may state that the actual ATF will seek those zero-crossings where the slope of the error function is positive. As a result, the first two operating modes of the actual ATF (for case I) are

$$b = 0; \quad 0 < |\sigma_o| \leq 0.250 \text{ msec} \qquad \text{(lowest mode)}$$

and

$$1.57 \text{ msec} \leq |b| \leq 1.65 \text{ msec} \qquad 0 < |\sigma_o| \leq 0.257 \text{ msec}.$$

Notice that the smallest total rms error is obtained when the ATF is operating in its lowest mode.

As to which mode the ATF will actually assume depends on the SNR and the initial bias conditions when the ATF is activated. Thus, it is very possible that at a high SNR and a large initial bias error the ATF will slip into the higher operating mode. However, as the SNR decreases, only the lowest operating mode is possible. This is evident from figure 11 since, as the horizontal line shifts upward, there will be no intersection with the curve representing b = 1.6 msec. Alternatively, since the BDI gain decreases as the bias increases (see figure 9), a point will be reached where equation (30) can no longer be satisfied unless the ATF slips into the lowest operating mode. Continuing with this reasoning, as the SNR decreases further, we note that a point will be reached where this lowest mode will also become unstable. This threshold point is indicated as point T in figures 8, 10, and 11. The various parameter values associated with this significant condition are

$$b = b_T = 0$$

$$\sigma_o = \sigma_T \cong 0.25 \text{ msec}$$

$$K_{BDI} = K_{BDI}\Big|_T = 0.717 \times 10^{10}$$

$$\frac{1}{G_{nn}} = \frac{1}{G_{nn}\Big|_T} = (SNR)_T = \frac{1}{0.0143}, \text{ or } (-18.46 \text{ dB}).$$

Thus, based on this graphic analysis and assuming that the ATF is operating in its lowest mode, the ATF will become unstable when the SNR approaches -18.46 dB. At the verge of threshold, the bias error will be zero, and the random error will be 0.25 msec.

Having determined the final threshold operating point, we can now choose α. Using equation (25) and the BDI gain at the threshold yields

$$\alpha = 3.137 \times 10^{-11} \text{ sec/volt}^2 .$$

Theoretically, this value of α ensures that under uncorrelated noise conditions the ATF will be able to follow a 40 knot moving target over its entire operating range with a lag error not exceeding 100 yd (91.44 m).

Once the system is calibrated (chosen α), it is possible to solve equation (30) or (17) for any other SNR. Indeed, once α has been determined, one may program equations (8) and (17) on a computer and initiate an automatic two-dimensional search for the steady-state solutions of the bias and random errors for any arbitrary acoustic conditions. The results of such an automated tracking program for uncorrelated noise are shown in figure 12 as a function of the SNR. Only the random error for the two lowest operating modes are shown. The bias error is, of course, zero for the lowest mode and varies between 1.57 and 1.63 msec for the 2nd order mode (see figure 8). Inspection of figure 12 shows that the threshold of the lowest order operating mode (thresholds) is at SNR = -18.6 dB and that the random error at this point is 0.28 msec. The reason that both of these values differ from the expected -18.46 dB and 0.25 msec, respectively, is that the automated program uses the exact equivalent bandwidth, Δfe (equation 22), rather than approximation (23), which was used in the previous graphic analysis. As expected, the 2nd order operating mode thresholds at a higher SNR (-16.5 dB) and exhibits a larger total rms error.

For comparison purposes, figure 12 also shows the Cramér-Rao lower bound (CRLB) for a two-element analog BDI followed by a 20 sec averager (open-loop tracker). The absolute values of the random errors cannot be compared directly because one curve pertains to a closed-loop ATF and the CRLB pertains to an open-loop ATF. What is significant, however, is the shape of the two curves. The figure shows that σ_0 is proportional to the theoretical variation over a large range of SNR:

$$\left[\frac{1 + 2\,(\text{SNR})}{(\text{SNR})^2}\right]^{1/2}$$

At a low SNR, the ATF exhibits the expected threshold; however, at a high SNR, the model gradually becomes invalid due to the assumption that $G_{NN}\,(0, m, \sigma^2)$ is independent of m and σ.

CASE II--SINGLE TARGET IN PARTIALLY CORRELATED NOISE

The conditions for case II are

$$\beta = 0, \quad I = 0,$$

so that equations (19)-(21) reduce to

$$G_{w_1w_1}(f) = G_{w_2w_2}(f) = 1 + G_{nn}$$
$$G_{w_1w_2}(f) = e^{-i2\pi f t_{s1}} + \gamma(f)\, G_{nn}. \tag{33}$$

These spectral densities may now be substituted into the appropriate expressions in the manner outlined for case I. When the previously determined value for α and a direct signal time delay of $t_{s1} = -0.2$ msec are employed, the bias and random errors are shown in figure 13 as a function of SNR, with the noise coherence (γ) as a parameter. For this case, the noise coherence is assumed to be real and independent of frequency.* Furthermore, only the results for the lowest operating mode are shown.

Notice, when comparing figures 13 and 12, that as the noise becomes partially correlated, the bias error increases substantially. As the SNR decreases, the ATF will tend to track the noise, which is effectively located at broadside. Eventually, the bias error approaches $(-t_{s1}) = 0.2$ msec. Note that for all SNR's, the random error is only a small fraction of the bias error. Although not shown in figure 13, the ATF will threshold at a lower SNR than when the noise is uncorrelated. For example, for $\gamma = 0.1$, the ATF will threshold at -32 dB.

---

*The reader is cautioned that the assumption of noise coherence, which is real and independent of frequency, is a highly artificial case and is not representative of real data. It was chosen here primarily to indicate a general trend that could be expected without becoming involved in any particular noise model.

CASE III--SINGLE TARGET IN UNCORRELATED NOISE PLUS INTERFERENCE

The conditions for case III are

$\beta = 0, \quad \gamma = 0,$

so that equation (19)-(21) reduce to

$$G_{w_1w_1}(f) = G_{w_2w_2}(f) = 1 + G_{II} + G_{nn}$$

$$G_{w_1w_2}(f) = e^{-i2\pi f t_{S1}} + G_{II}\, e^{-i2\pi f t_I} . \tag{34}$$

Figure 14 shows the bias and random errors as a function of t_I for the following parameter values:

$t_{S1} = 0$ (target at broadside)

t_I varies form 0 to 1.6 msec

$G_{II} = 2.5$ (interference is 2.5 times as intense as the signal)

$G_{nn} = 6.32$ (SNR = -8 dB)

Also, for each value of t_I, the automatic search routine was initiated at the true target's time delay, that is, at b = 0

Before discussing figure 14 further, it should be noted that the resultant error function for this case is the sum of the error function due to the true target (as shown in figure 7) and to the interfering target (2.5 times as large as that shown in figure 7 and shifted to the right by t_I). In light of the discussion concerning case I, the ATF, when operated in its lowest mode, will seek the zero-crossing of the resultant error function having the smallest bias error and a positive slope.

The ATF in figure 14 will settle on a time delay situated between the true target and the interfering target. Indeed, it may be shown that for small t_I the resultant bias error is approximately given by

$$b \approx \left(\frac{G_{II}}{1 + G_{II}}\right) t_I \quad \text{for} \leq 0 \quad t_I < 0.4 \text{ msec.}$$

As t_I increases further, this linear relationship will no longer hold and the bias error will almost approach t_I. Then, in the vicinity of $t_I \approx 0.8$ msec, the bias error abruptly changes sign due to the effect of the first "side lobe" of the interference error function. Eventually, the bias error smoothly decreases to zero as t_I approaches 1.58 msec, at which point a null occurs in the error function because of the interfering target. It is important to note that the discontinuity in the bias error depends on the search routine and on the initial bias error. If, for example, the automatic search routine were initiated at a delay time in the vicinity of t_I, the ATF would have continued to track the interference and no discontinuity would have occurred. As t_I increases from 1.58 to 2.72 msec, the bias error also exhibits a cyclic behavior. The maximum excursions are considerably smaller, however, since the 2nd side lobe of the interference error function is smaller. There is no discontinuity in this region because the slope of the resultant error function remains positive in the vicinity of the origin. Also notice that, as for case II, the random error is only a small fraction of the bias error.

CASE IV--SINGLE TARGET WITH MULTIPATH IN UNCORRELATED NOISE

The simple, but practical, multipath example considered for case IV is shown in figure 15. In that figure, the two-element array is situated at a fixed depth (D_1), whereas the target, which is located at a fixed range (R and angle, Θ with respect to the array normal), varies in depth from 200 to 1000 ft (60.96 to 304.80 m). The acoustic signal impinging upon the array arrives via a direct path and a surface-reflected path. The problem is to determine the bias and random errors as a function of the target depth for various angles of Θ.

From the geometry, one may readily compute the required parameters listed on pages 8 and 9:

$$t_0 = t_{OS1} - t_{OS2} = \frac{L_{OS1} - L_{OS2}}{C}$$

$$\left.\begin{aligned} \tau_{S1} &= \frac{d}{C}\ \frac{R\sin\theta}{L_{OS1}} \\ t_{S2} &= \frac{d}{C}\ \frac{R\sin\theta}{L_{OS2}} \end{aligned}\right\} \text{ for } R >> d,$$

where

$L_{OS1} = \left[R^2 + (D_1 - D_2)^2\right]^{1/2}$ length of the direct path

$L_{OS2} = \left[R^2 + (D_1 + D_2)^2\right]^{1/2}$ length of the reflected path

D_1 = depth of the array

D_2 = depth of the target

d = sensor spacing

Further particulars assumed for this case are

$\beta = -\frac{L_{OS1}}{L_{OS2}}$ (negative due to the 180^o phase shift at the surface reflection)

C = 4850 ft/sec (1478.28 msec)

d = 3.692 ft (1.1253 m)

D_1 = 600 ft (182.88 m)

R = 3000 ft (914.40 m)

I = 0 (no interference)

γ = 0 (noise uncorrelated)

G_{nn} = 6.32 (SNR = -8 dB)

The result of simultaneously solving equations (8) and (17) for the bias and random errors is shown in figure 16. It will be noted that the random error is essentially the same for the three angles

illustrated. This is merely a further demonstration of the fact that equations (8) and (17) are only loosely coupled at small bias and small random errors. The bias error is, of course, zero only when the target is at broadside ($\Theta = 0$) and increases smoothly as Θ increases. The magnitude remains relatively small, however, because the difference between L_{OS1} and L_{OS2} is small.

CONCLUSIONS

It has been shown that the straightforward application of simple control theory to a linearized model of an analog BDI results in two coupled transcendental equations whose unknowns are the mean and the variance of the controlling time delay. The unique feature of this analysis is that, from the outset, this time delay is treated as a random variable (Gaussian) and that the BDI is linearized about an arbitrary operating point. This ensures that the resulting expressions remain valid at large rms errors and allows investigation of the ATF performance in the vicinity of the threshold.

It was also shown that a more complete expression for the BDI gain is one that involves the total variation of the average BDI output, that is, the variation with respect to the mean and the standard deviation of the controlling time delay.

The utility of this analytical approach has been demonstrated by solving the coupled mean and variance expressions for split-beam ATF operating in four adverse acoustic environments. Particular emphasis was place on case I (Single Target in Uncorrelated Noise) since this afforded a simple example of the calibration procedure of the effective time constant of the closed-loop filter, as well as of the identification of stable operating modes.

This analysis has shown that the estimator is unbiased only when the ATF is operating in its lowest order mode, and that the variation of the random error with the SNR is identical to that predicted by the Cramér-Rao lower bound over most of its operating range. At -18.6 dB, the ATF exhibits the expected threshold, whereas at an SNR in excess of approximately +4 dB the ATF exhibits slightly higher random errors. As the noise becomes partially correlated, the bias error increases sharply and is considerably larger than the random error. As expected, at low SNR, the ATF tracks the noise, which is effectively located at broadside.

Cases III and IV (Single Target in Uncorrelated Noise Plus Interference and Single Target with Multipath in Uncorrelated Noise, respectively) show the effect of an interfering target and multipath. These cases were included primarily to demonstrate the general usefulness of the derived expressions.

It should be mentioned again that the work in this report was confined to a two-element array in order to focus on the ATF analysis, and may readily be extended to include any array geometry by proper modification of the equations in appendix A.

Indeed, the computer program mentioned in the text is actually written for an unshaded 50 element equally spaced array. With proper scaling to the effective half-beam centers, the primary effect of this array is to decrease the height of the "side lobes" of the error function. Consequently, the results for case I remain essentially unchanged (except for the increased SNR), whereas the effect of an interfering target is decreased considerably from that indicated in case III even after proper scaling.

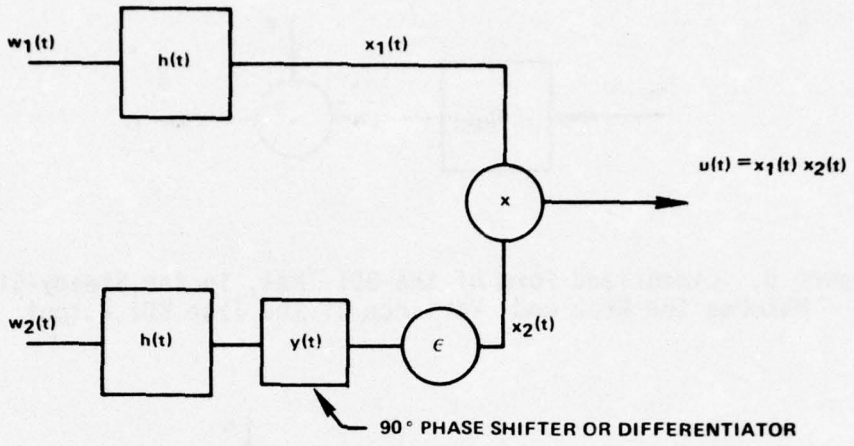

Figure 1. A BDI

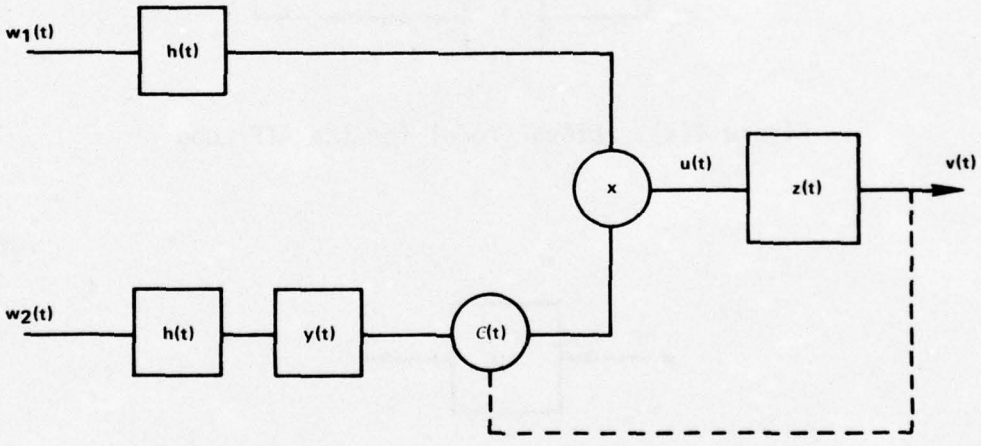

Figure 2. An Analog ATF

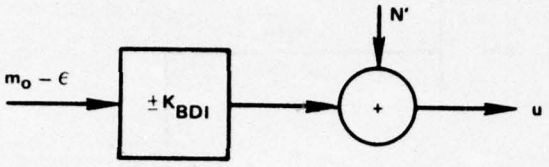

Figure 3. Linearized Form of the BDI That, in the Steady-State, Matches the Mean and Variance of the True BDI Output

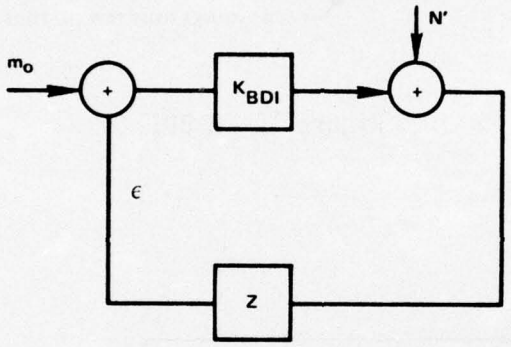

Figure 4(a). Linear Model for the ATF Loop

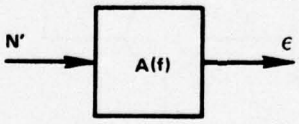

Figure 4(b). Equivalent Filter Relating N' and ϵ

Figure 4. Model for Determining the Closed-Loop Filter

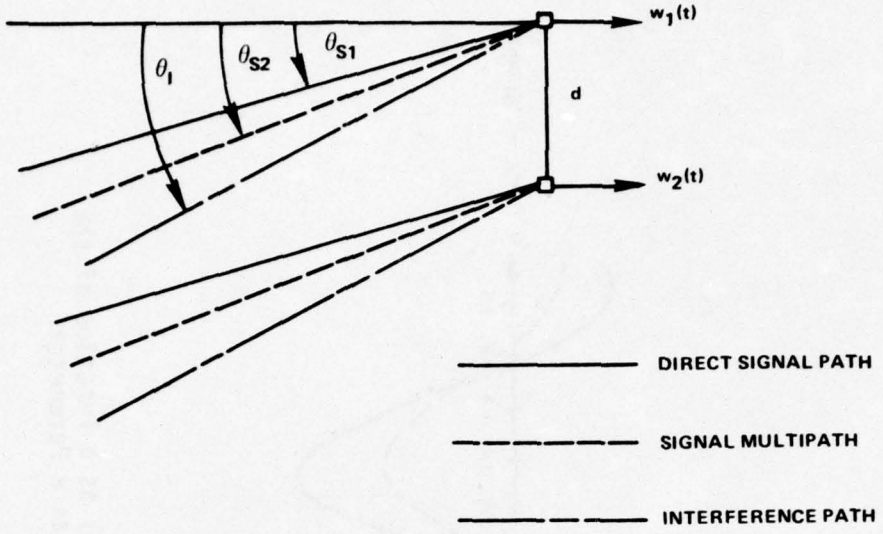

Figure 5. Geometry of the Two-Sensor Array

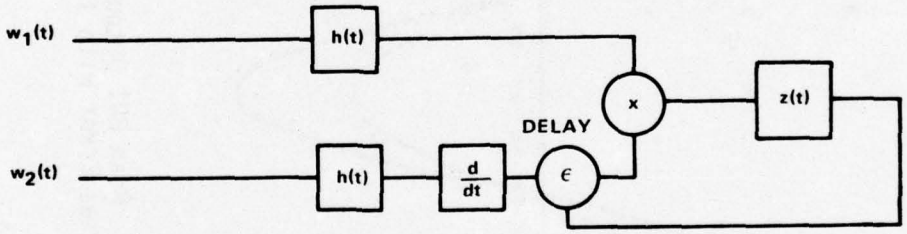

Figure 6. Analog ATF Used for the Examples

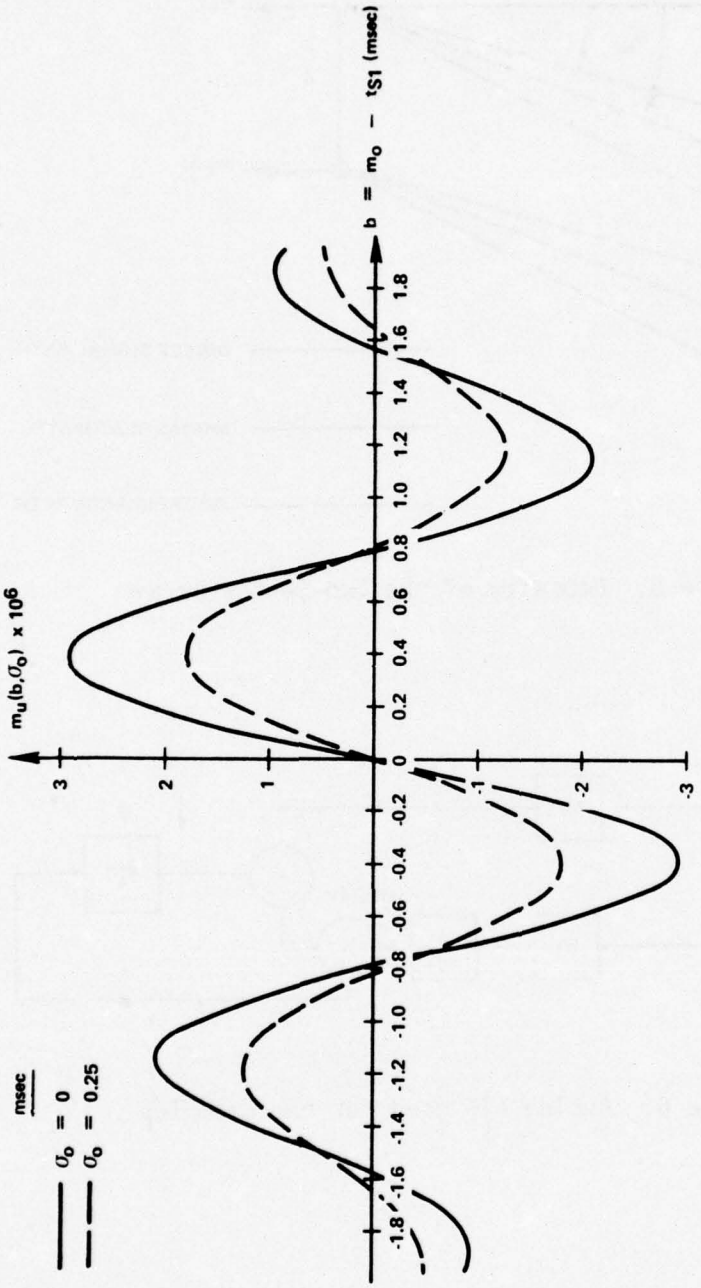

Figure 7. Mean BDI Output (Error Function) as a Function of the Bias Error With Time-Delay Jitter as a Parameter

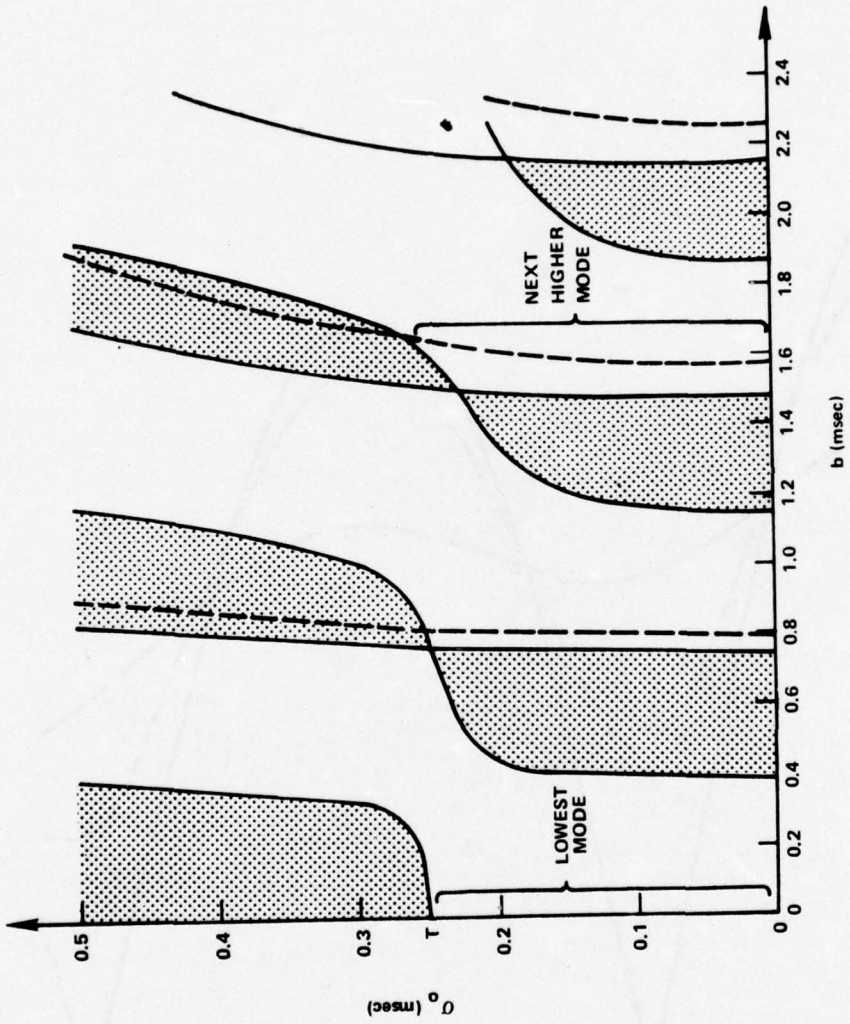

Figure 8. Stability Diagram of the ATF Under Uncorrelated Noise Conditions

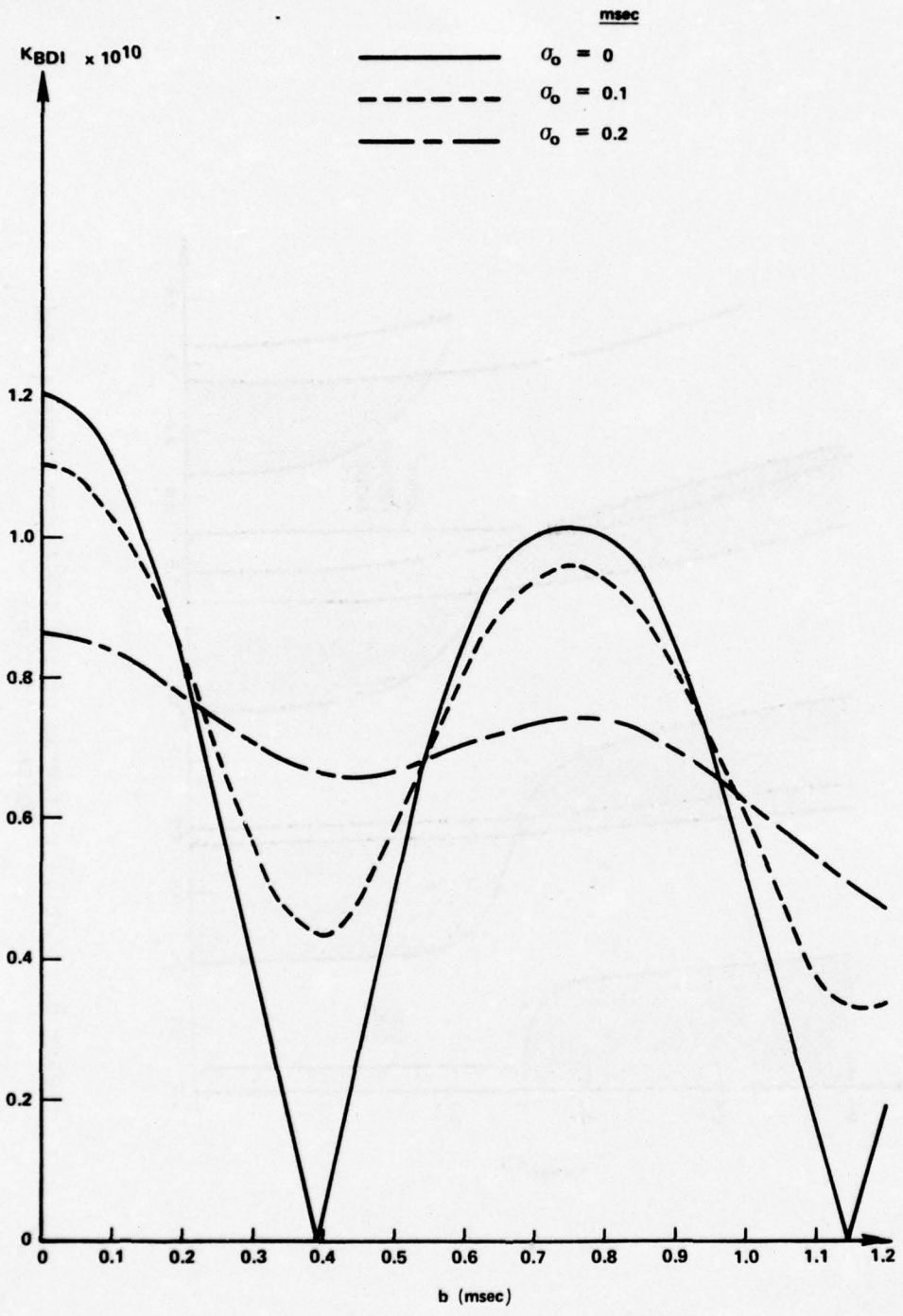

Figure 9. BDI Gain as a Function of the Bias Error With Time-Delay Jitter as a Parameter

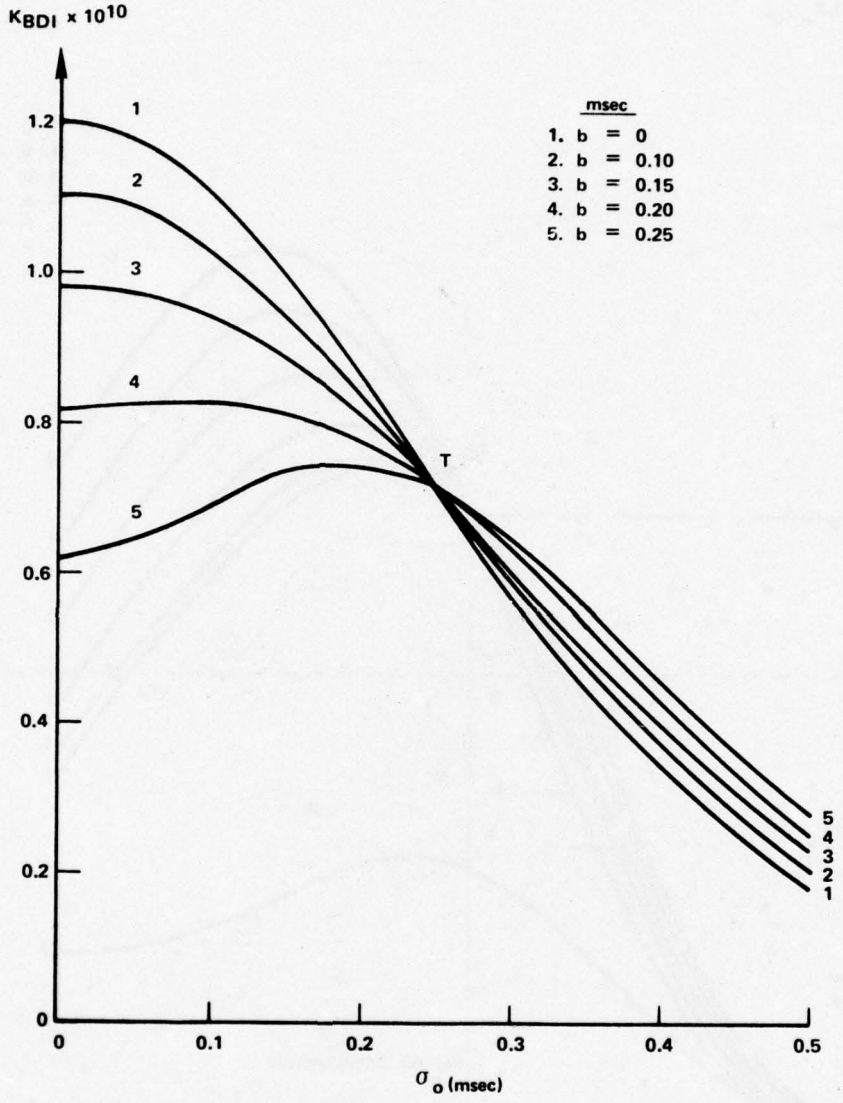

Figure 10. BDI Gain as a Function of the Time-Delay Jitter With Bias Error as a Parameter

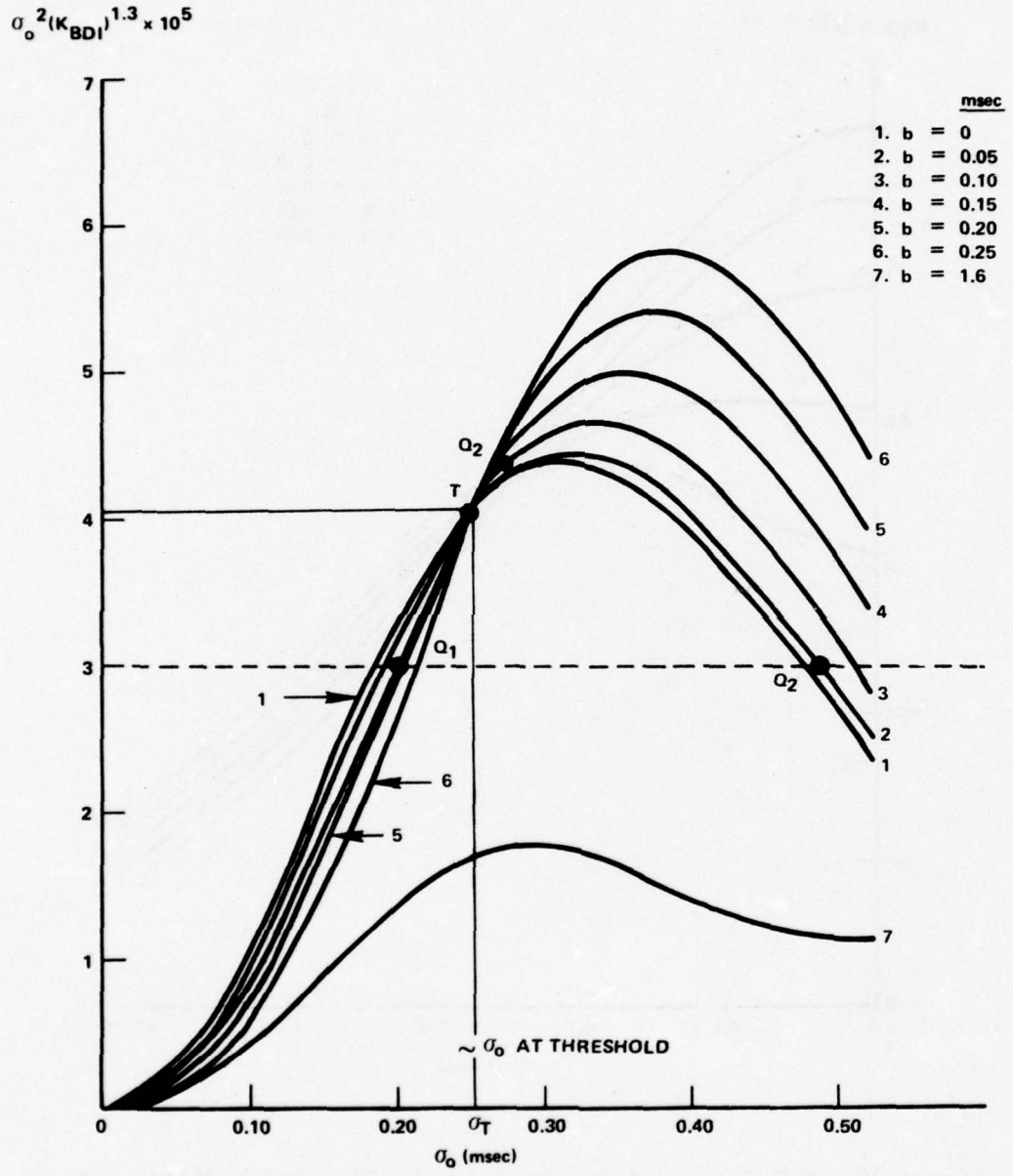

Figure 11. Graphical Solution to the Transcendental Equation Resulting from the Variance Expression

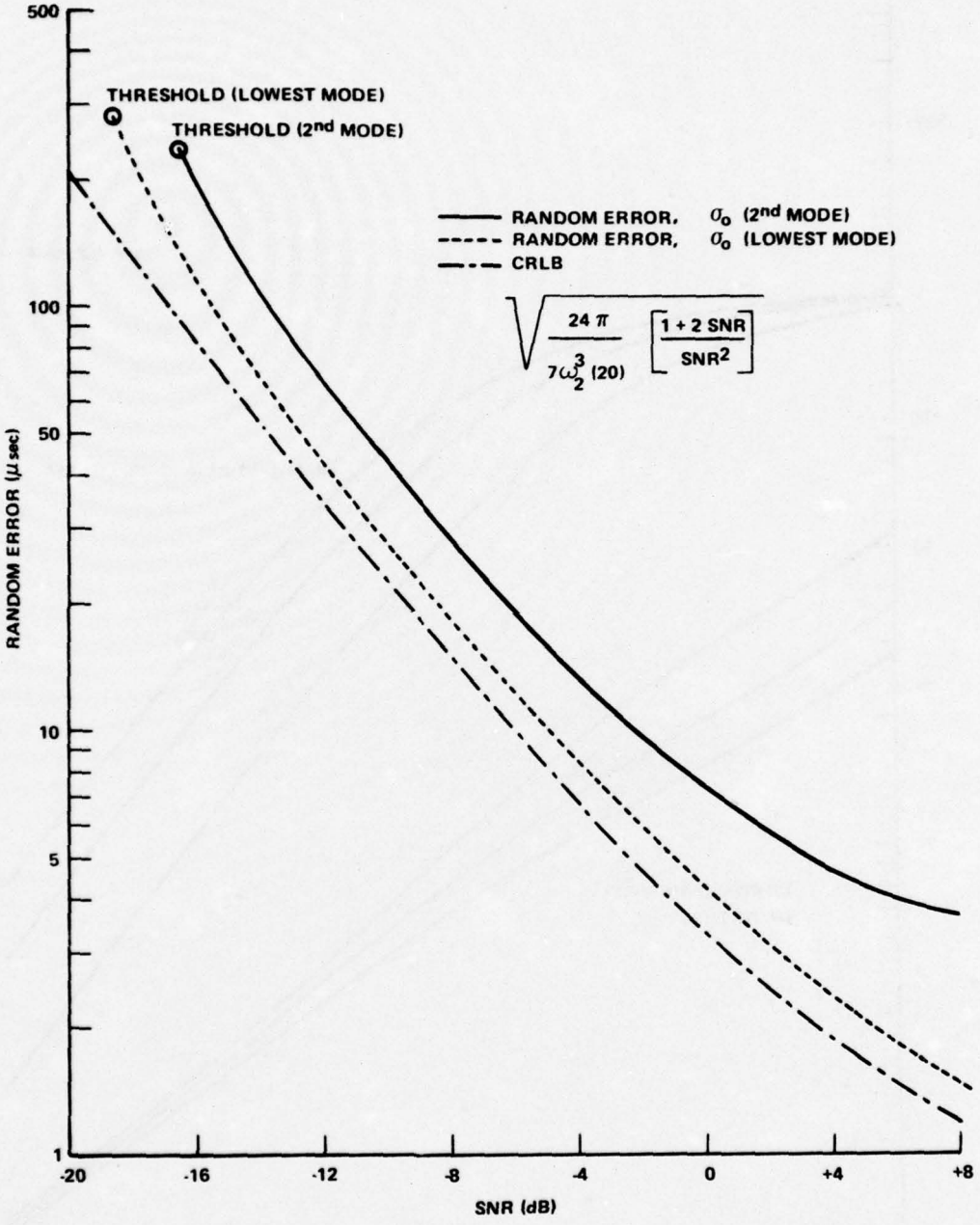

Figure 12. Steady-State Random Error of the ATF in its Two Lowest Operating Modes as a Function of SNR

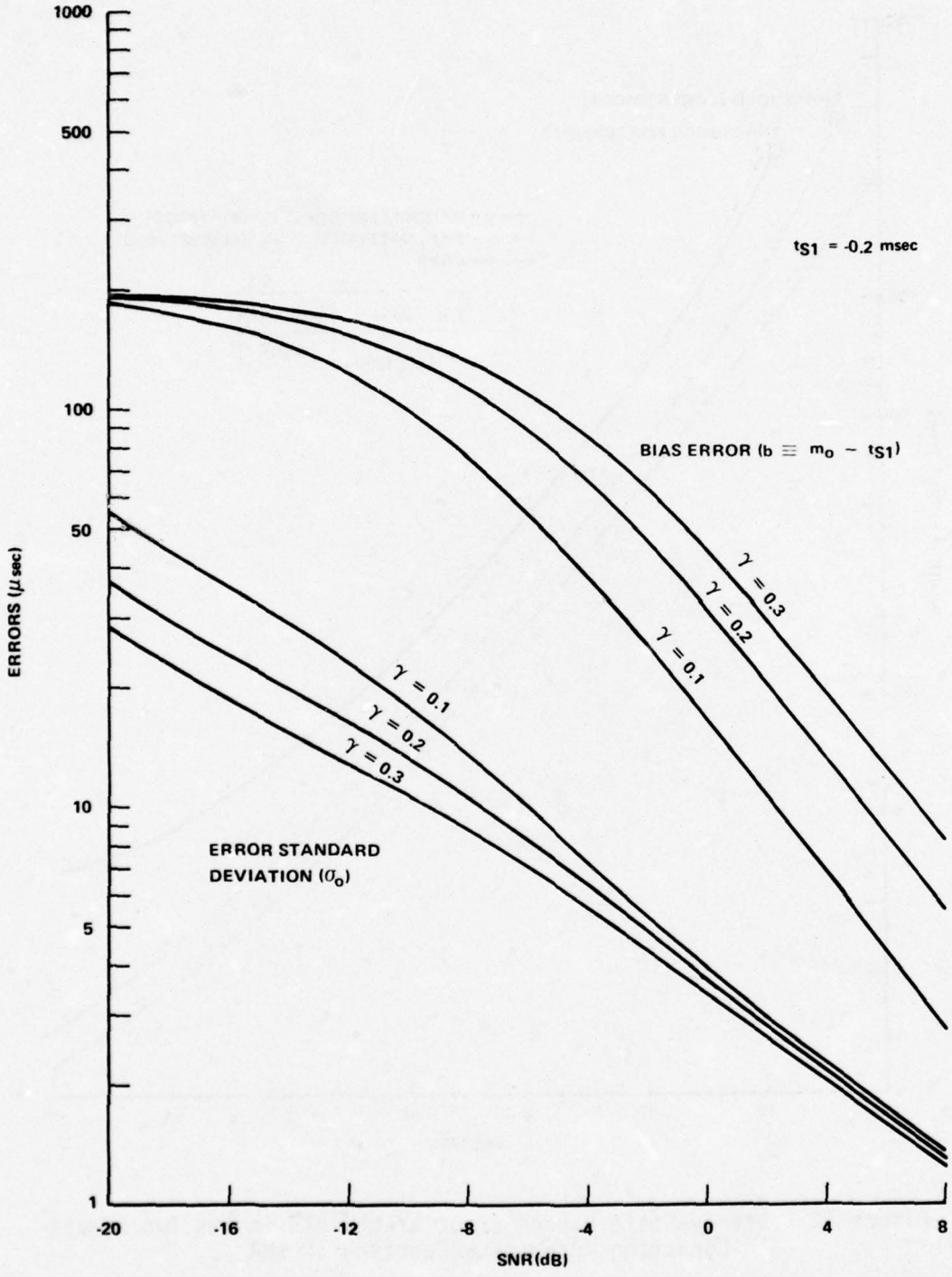

Figure 13. Bias and Random Errors of the ATF Under Partially Correlated Noise Conditions

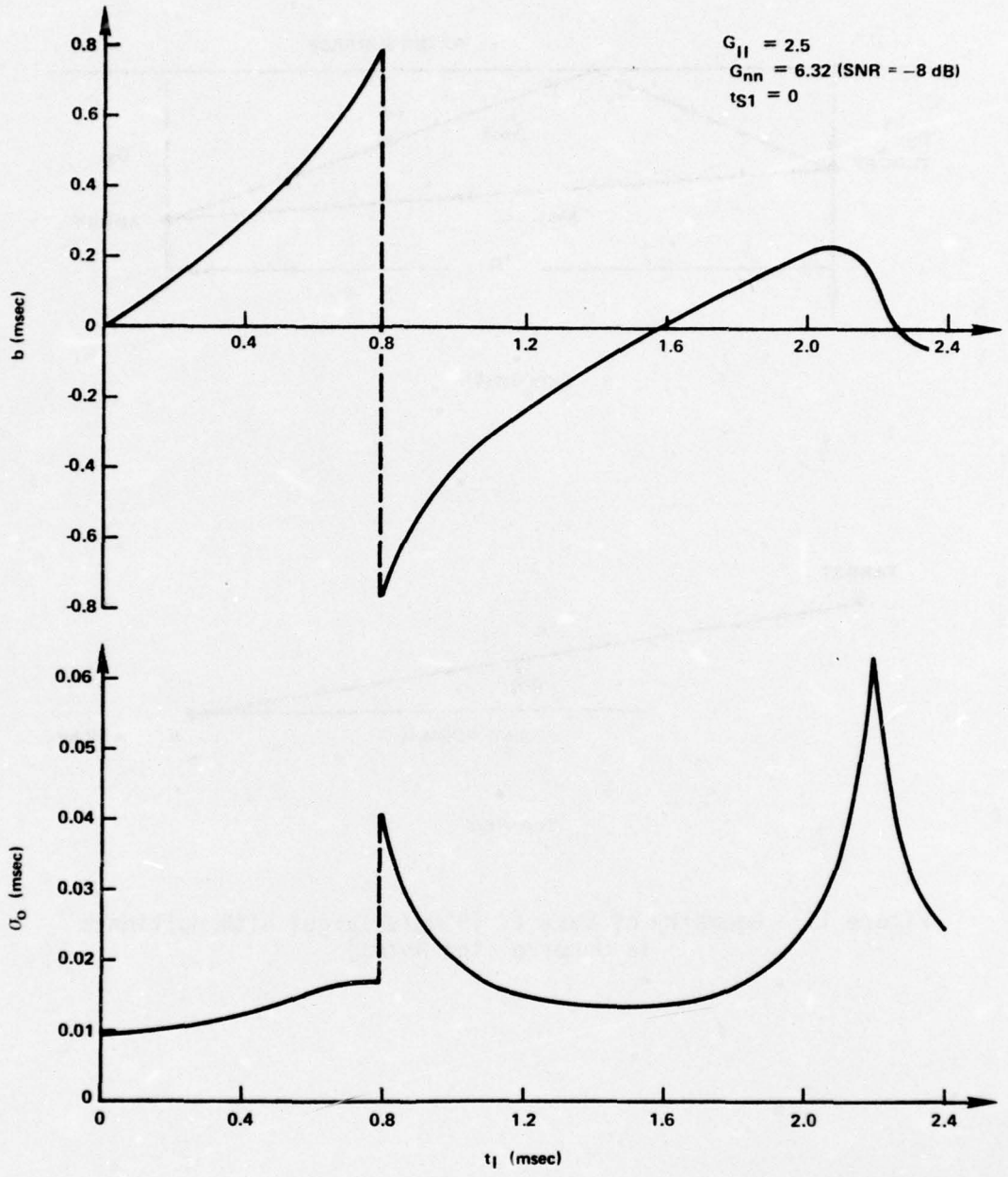

Figure 14. Bias and Random Errors of the ATF due to a Moving Interference

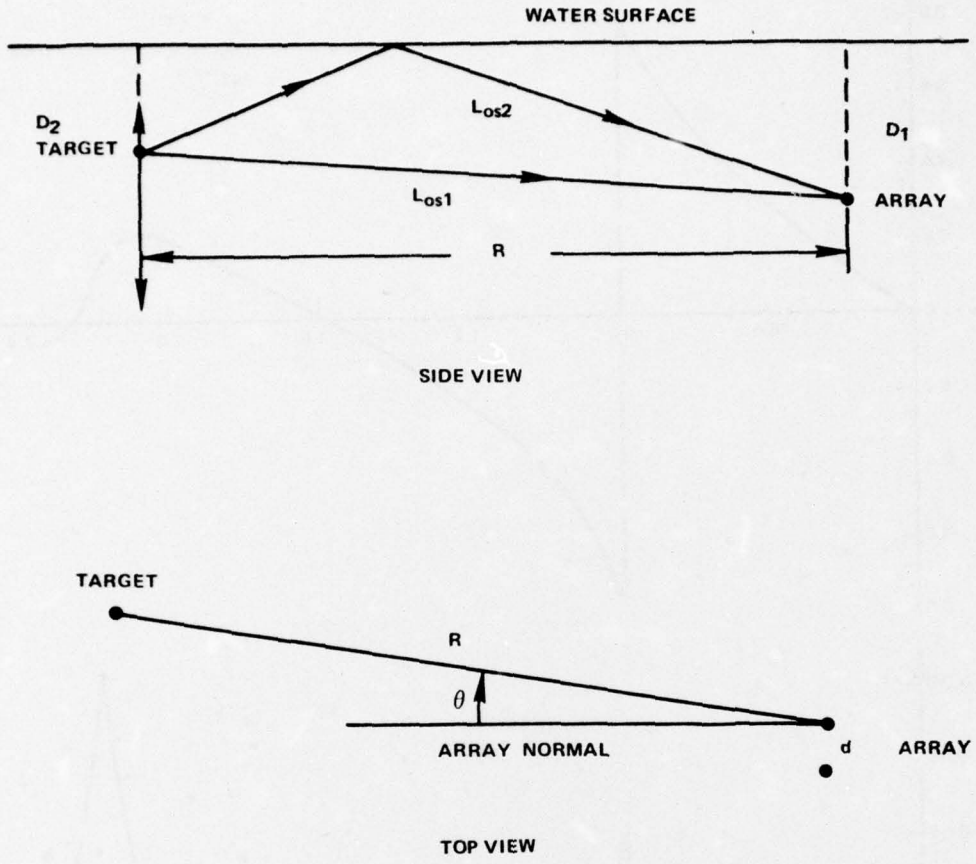

Figure 15. Geometry of Case IV (Single Target With Multipath in Uncorrelated Noise)

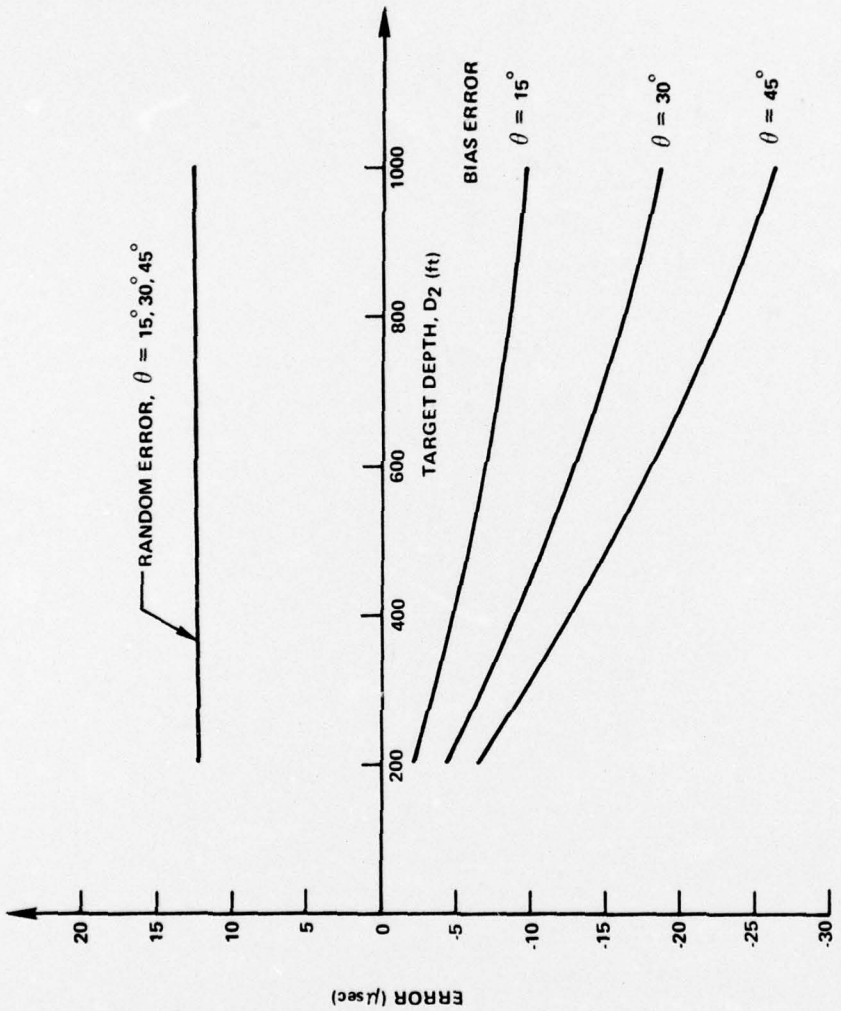

Figure 16. Steady-State Bias and Random Errors for Case IV Depicted in Figure 15

REFERENCES

1. V. H. MacDonald and P. M. Schultheiss, "Optimum Passive Bearing Estimation in a Spatially Incoherent Noise Environment," Progress Report 37, in Processing of Data From Sonar Systems, vol. VI, General Dynamics/Electric Boat Division, Groton, Connecticut, 1 September 1968, pp. C-1 -- C-42.

2. V. H. MacDonald, "Optimum Passive Bearing Estimation in a Spatially Coherent Noise Environment," Progress Report 40, in Processing of Data From Sonar Systems, vol. VII, General Dynamics/Electric Boat Division, Groton, Connecticut, 11 August 1970, pp. C-1 -- C-28.

3. P. M. Schultheiss, "Some Comments on Optimum Bearing Estimation," Progress Report 32, in Processing of Data From Sonar Systems, vol. V, supplement I, General Dynamics/Electric Boat Division, Groton, Connecticut, 31 July 1968, pp. B-1 -- B-32.

4. P. M. Schultheiss, Sensitivity of Bearing Estimates to Noise Field Statistics, Yale University Department of Engineering and Applied Science, New Haven, Connecticut, February 1975 (NUSC Contract N66604-74-0525).

5. An Analytical Study of Factors Limiting Automatic Target Following Operation with Passive Sonar Equipment at Low Acoustic Signal-to-Noise Ratios, Final Report, ATF Study, (FR180 Report), vol. I, Raytheon Company, Submarine Signal Operation, Portsmouth, Rhode Island, 16 March 1962.

6. A. G. Lindgren and R. F. Pinkos, Analysis and Design of Passive Sonar Tracking Systems, Report 417-03, University of Rhode Island, Kingston, Rhode Island, June 1968.

7. R. F. Pinkos and A. G. Lindgren, Passive Angle Tracking Systems Report 4005-04, Naval Underwater Weapons Research and Engineering Station, Newport, Rhode Island, September 1969.

8. J. A. Develet, Jr., "A Threshold Criterion for Phase-Lock Demodulation," Proceedings of the IEEE, vol. 51, no. 2, February 1963, pp. 349-356.

Appendix A

THE MEAN AND VARIANCE OF THE BDI

The mean and the variance of the output of the processor shown in figure 1 are derived here. This is accomplished by first computing the relevant conditional expectations and then averaging them over the random time delay (ε).

In figure 1, the Fourier transform of the composite filter in channel 1 is

$$H_1(f) = H(f) \tag{A-1}$$

and in channel 2 is (at a given ε)

$$H_2(f) = H(f)\, Y(f) e^{-i2\pi f\varepsilon}. \tag{A-2}$$

The auto- and cross-spectral densities of $x_1(t)$ and $x_2(t)$ may then be expressed as

$$G_{x_1x_1}(f) = |H_1(f)|^2 G_{w_1w_1}(f) = |H(f)|^2 G_{w_1w_1}(f) \tag{A-3}$$

$$G_{x_2x_2}(f) = |H_2(f)|^2 G_{w_2w_2}(f) = |H(f)|^2 |Y(f)|^2 G_{w_2w_2}(f) \tag{A-4}$$

$$G_{x_1x_2}(f,\varepsilon) = H_1(f)H_2^*(f)\, G_{w_1w_2}(f) = |H(f)|^2 Y^*(f)\, G_{w_1w_2}(f) e^{i2\pi f\varepsilon}, \tag{A-5}$$

where $G_{w_1w_1}(f)$ and $G_{w_2w_2}(f)$ are the auto-spectral densities and $G_{w_1w_2}(f)$ is the cross-spectral density of the input sample functions. It should be noted that only the cross-spectral density $G_{x_1x_2}(f,\varepsilon)$ depends on the delay (ε).

For algebraic convenience, the following definitions shall be made:

$$\phi_1(f) \equiv |H(f)|^2 \, G_{w_1 w_1}(f) = G_{x_1 x_1}(f) \tag{A-6}$$

$$\phi_2(f) \equiv |H(f)|^2 \, |Y(f)|^2 \, G_{w_2 w_2}(f) = G_{x_2 x_2}(f) \tag{A-7}$$

$$\phi_{12}(f) \equiv |H(f)|^2 \, Y^*(f) \, G_{w_1 w_2}(f) = G_{x_1 x_2}(f,\varepsilon) e^{-i2\pi f\varepsilon}. \tag{A-8}$$

The conditional expectation of the output u(t) may now be determined. At a given ε,

$$\overline{u(t)} = E(u|\varepsilon) = \overline{x_1(t) \, x_2(t)} = R_{x_1 x_2}(0) = \int G_{x_1 x_2}(f,\varepsilon) df, \tag{A-9}$$

where the fact that $R_{x_1 x_2}(\tau)$ and $G_{x_1 x_2}(f)$ are a Fourier transform pair has been used. The conditional expectation averaged over the probability density ($p(\varepsilon)$) of ε will then yield the average output (m_u). Thus,

$$m_u = E(u) = \int d\varepsilon \; p(\varepsilon) \; E(u|\varepsilon) = \iint d\varepsilon \; df \; p(\varepsilon) \; G_{x_1 x_2}(f,\varepsilon). \tag{A-10}$$

Substituting for $G_{x_1 x_2}(f,\varepsilon)$ and integrating over ε yields

$$m_u = \int \phi_{12}(f) \; C(2\pi f) df \tag{A-11}$$

$$m_u = \int |H(f)|^2 \, Y^*(f) \, G_{w_1 w_2}(f) \, C(2\pi f) df, \tag{A-12}$$

where

$$C(2\pi f) \equiv \int e^{i2\pi f\varepsilon} \; p(\varepsilon) d\varepsilon \tag{A-13}$$

is the characteristic function of the random variable (ε).

The conditional expectation of $u^2(t)$ may be computed in a similar fashion. For this purpose, it is necessary to evaluate $\overline{u(t)\ u(t-\tau)}$. Using the Gaussian property of the input sample functions, one may write

$$\overline{u(t)\ u(t-\tau)} = R_{uu}(\tau) = \overline{x_1(t)\ x_2(t)\ x_1(t-\tau)\ x_2(t-\tau)} \tag{A-14}$$

$$R_{uu}(\tau) = R^2_{x_1x_2}(0) + R_{x_1x_1}(\tau)R_{x_2x_2}(\tau) + R_{x_1x_2}(\tau)R_{x_2x_1}(\tau). \tag{A-15}$$

Taking the Fourier transform yields

$$G_{uu}(f,\varepsilon) = R^2_{x_1x_2}(0)\ \delta(f) + G_{x_1x_1}(f) \circledast G_{x_2x_2}(f) + G_{x_1x_2}(f,\varepsilon) \circledast G^*_{x_1x_2}(f,\varepsilon), \tag{A-16}$$

where $\circledast$ denotes convolution.

The conditional expectation of $u^2(t)$ may now be obtained as follows:

$$E(u^2|\varepsilon) = R_{uu}(0) = \int G_{uu}(f,\varepsilon)df \tag{A-17}$$

$$E(u^2|\varepsilon) = E^2(u|\varepsilon) + \int df\left[G_{x_1x_1}(f) \circledast G_{x_2x_2}(f) + G_{x_1x_2}(f,\varepsilon) \circledast G^*_{x_1x_2}(f,\varepsilon)\right] \tag{A-18}$$

since, from equation (A-9), $R_{x_1x_2}(0) = E(u|\varepsilon)$.

The variance of u may be obtained from the following relation:

$$\sigma_u^2 \equiv \mathrm{var}(u) = E(u^2) - E^2(u)$$

$$\sigma_u^2 = \int d\varepsilon\ p(\varepsilon)\ E(u^2|\varepsilon) - E^2(u). \tag{A-19}$$

Substituting equation (A-18) into (A-19) yields

$$\sigma_u^2 = \left[\int d\varepsilon\ p(\varepsilon)\ E^2(u|\varepsilon) - E^2(u)\right]$$
$$+ \iint df d\varepsilon\ p(\varepsilon)\left[G_{x_1x_1}(f) \circledast G_{x_2x_2}(f)\right.$$
$$\left. + G_{x_1x_2}(f,\varepsilon) \circledast G^*_{x_1x_2}(f,\varepsilon)\right] .$$

Finally, substituting equations (A-6)-(A-9) into the above expression and integrating over ε yields

$$\sigma_u^2 = \iint df_1 df_2\ \phi_{12}(f_1)\ \phi_{12}(f_2)\ \left\{C[2\pi(f_1 + f_2)] - C(2\pi f_1)\ C(2\pi f_2)\right\}$$
$$+ \int G_{NN}(f)df, \qquad \text{(A-20)}$$

where

$$G_{NN}(f) \equiv \phi_1(f) \circledast \phi_2(f) + \int dx\ \phi_{12}(x)\ \phi_{12}(x - f)\ \ C[2\pi(2x - f)]. \qquad \text{(A-21)}$$

A moment of reflection will reveal that the spectral density $G_{NN}(f)$ is the average (averaged over ε) auto-spectral density of a random variable (N), which, at a <u>given</u> ε, is equal to $(u - \bar{u})$.

Equations (A-11) and (A-20) represent the desired expressions for a general random time delay (ε). Any additional simplification of these results requires further assumptions. Consider, for example, that ε is deterministic and has the value ε_o. In this limiting case, the probability density of ε assumes the form $p(\varepsilon) = \delta(\varepsilon - \varepsilon_o)$; and the characteristic function of ε becomes

$$C(\eta) = \int d\varepsilon\ \ \delta(\varepsilon - \varepsilon_o)e^{i\eta\varepsilon} = e^{i\eta\varepsilon_o}.$$

It is immediately apparent that the first term in equation (A-20) vanishes. (Hence, this term arises due to the randomness of ε.) The complete expressions under this condition are

$$m_u = \int df\ \phi_{12}(f)\ e^{i2\pi f\varepsilon_o}$$

$$\sigma_u^2 = \int df \left[\phi_1(f) \circledast \phi_2(f) + \phi_{12}(f)\ e^{i2\pi f\varepsilon_o} \circledast \phi_{12}^*(f)\ e^{-i2\pi f\varepsilon_o}\right]. \tag{A-22}$$

Another interesting simplification results if the random time delay (ε) has a Gaussian probability density with a mean (m) and a variance (σ^2). Then, the characteristic function becomes

$$C(\eta) = e^{i\eta m}\ e^{-1/2(\eta\sigma)^2}. \tag{A-23}$$

The term in the brackets in equation (A-20) may be expanded as follows:

$$\left\{C\left[2\pi(f_1 + f_2)\right] - C(2\pi f_1)\ C(2\pi f_2)\right\} = \left[e^{-(2\pi\sigma)^2 f_1 f_2} - 1\right]$$

$$\cdot\left[e^{i2\pi f_1 m}\ e^{-1/2(2\pi f_1\sigma)^2}\right]\ \left[e^{i2\pi f_2 m}\ e^{-1/2(2\pi f_2\sigma)^2}\right]$$

$$\{\ \} = \left[e^{i2\pi f_1 m}\ e^{-1/2(2\pi f_1\sigma)^2}\right]\ \left[e^{i2\pi f_2 m}\ e^{-1/2(2\pi f_2\sigma)^2}\right]$$

$$\sum_{n=1}^{\beta} \frac{(i2\pi f_1\sigma)^n\ (i2\pi f_2\sigma)^n}{n!}, \tag{A-24}$$

where the series expansion for the exponential $e^{-(2\pi\sigma)^2 f_1 f_2}$ has been used. As a result, the first term of the variance expression (A-20) becomes

$$\sum_{n=1}^{\infty} \frac{\sigma^{2n}}{n!} \left[\int df (i2\pi f)^n \, \phi_{12}(f) \, e^{i2\pi fm} \, e^{i2\pi f\sigma)^2} \right]^2 . \qquad \text{(A-25)}$$

However, the term within the brackets is nothing more than the n-th derivative with respect to m of m_u, as the reader may readily verify by substituting equation (A-23) into (A-11) and differentiating. Consequently, the complete expressions for a Gaussian random delay (ε) become

$$m_u = \int df \, \phi_{12}(f) \, e^{i2\pi fm} \, e^{-1/2(2\pi f\sigma)^2} \qquad \text{(A-26)}$$

$$\sigma_u^2 = \sum_{n=1}^{\infty} \frac{\sigma^{2n}}{n!} \left(\frac{\partial^n m_u}{\partial m^n} \right)^2 + \int G_{NN}(f) df, \qquad \text{(A-27)}$$

where

$$G_{NN}(f) = \phi_1(f) \circledast \phi_2(f) + \int dx \, \phi_{12}(x) \, \phi_{12}(x - f) \, e^{i2\pi m(2x - f)} \cdot e^{-1/2[2\pi\sigma(2x - f)]^2}. \qquad \text{(A-28)}$$

Appendix B

LINEARIZATION OF THE VARIANCE OF THE BDI OUTPUT

The variance of the BDI output, as given by equation (2) or (A-27), is expanded here about some unspecified operating point at m_o and σ_o. For this purpose, a number of definitions and assumptions are made. Recall that the mean of the BDI output (m_u) is given by (see A-26)

$$m_u(m,\sigma^2) = \int df\ \phi_{12}(f)\ \ e^{i2\pi fm}\ \ e^{-1/2(2\pi f\sigma)^2}. \tag{B-1}$$

Now, if one defines $K_n(m,\sigma^2)$ as

$$K_n(m,\sigma^2) \equiv \frac{\partial^n}{\partial m^n}\ \left[m_u(m,\sigma^2)\right], \tag{B-2}$$

then the variance of the BDI output may be written as

$$\sigma_u{}^2(m,\sigma^2) = \sigma^2K_1^2 + \frac{1}{2!}\ \sigma^4\ K_2^2 + \frac{1}{3!}\ \sigma^6K_3^2 + \ldots$$

$$+\int G_{NN}(f,m,\sigma^2)df. \tag{B-3}$$

By numerically computing the higher order K's, as well as $G_{NN}(f,m,\sigma^2)$, we can see that within the expected operating range of the ATF the infinite series is accurately represented by the first two terms, and G_{NN} is relatively independent of m and σ. The latter is particularly true at low SNR's. Hence, a good approximation of equation (B-3) is

$$\sigma_u{}^2(m,\sigma^2) \approx \sigma^2K_1^2 + \frac{1}{2}\sigma^4\ K_2^2 + \int G_{NN}(f,m,\sigma^2)df. \tag{B-4}$$

Considering the variables to be m and σ^2, the above relationship may be expanded about the operating point at m_o and σ_o to yield

$$\sigma_u^2(m,\sigma^2) \approx \sigma_u^2(m_o,\sigma_o^2) + (m - m_o)\left(\frac{\partial\sigma_u^2}{\partial m}\right)_{m_o,\sigma_o}$$

$$+ (\sigma^2 - \sigma_o^2)\left[\frac{\partial\sigma_u^2}{\partial(\sigma^2)}\right]_{m_o,\sigma_o} \qquad \text{(B-5)}$$

Using the notation that K_{no} is the n-th derivative of m_u with respect to m evaluated at the operating point at m_o and σ_o, we note that the derivatives in equation (B-5) may be expressed as

$$\left(\frac{\partial\sigma_u^2}{\partial m}\right)_{m_o,\sigma_o} = 2\sigma_o^2 K_{10} K_{20} + \sigma_o^4 K_{20} K_{30} \qquad \text{(B-6)}$$

$$\left[\frac{\partial\sigma_u^2}{\partial(\sigma^2)}\right]_{m_o\sigma_o} = K_{10}^2 + 2\sigma_o^2 K10\left(\frac{\partial K_1}{\partial\sigma^2}\right)_{m_o,\sigma_o}$$

$$+ K_{20}^2 \sigma_o^2 + \sigma_o^4 K_{20}\left(\frac{\partial K_2}{\partial\sigma^2}\right)_{m_o,\sigma_o}, \qquad \text{(B-7)}$$

where the fact that G_{NN} is constant with respect to m and σ has been used. By using equations (B-1) and (B-2), we see that for all m and σ

$$\frac{\partial K_1}{\partial(\sigma^2)} = \frac{1}{2}K_3 \quad \text{and} \quad \frac{\partial K_2}{\partial(\sigma^2)} = \frac{1}{2}K_4.$$

Thereby, equations (B-6) and B-7) become

$$\left(\frac{\partial \sigma_u^2}{\partial m}\right)_{m_o,\sigma_o} = \sigma_o^2 K_{20}(2K_{10} + \sigma_o^2 K_{30}) \approx 2\sigma_o^2 K_{10}K_{20} \qquad \text{(B-8)}$$

$$\left[\frac{\partial \sigma_u^2}{\partial(\sigma^2)}\right]_{m_o,\sigma_o} = K_{10}(K_{10} + \sigma_o^2 K_{30}) + \sigma_o^2 K_{20}(K_{20} + \tfrac{1}{2}\sigma_o^2 K_{40})$$

$$\approx K_{10}^2 + \sigma_o^2 K_{20}^2 , \qquad \text{(B-9)}$$

where the approximations follow since $K_1 >> \sigma^2 K_3$ and $K_2 >> \sigma^2 K_4$ within the operating range. Substituting equations (B-8) and (B-9) and $\sigma_u^2(m_o,\sigma_o^2)$ into (B-5) yields

$$\sigma_u^2(m,\sigma^2) \approx \sigma_o^2 K_{10}^2 + \tfrac{1}{2}\sigma_o^4 K_{20}^2 + \int G_{NN}(f,m,\sigma_o^2)df \qquad \text{(B-10)}$$

$$+ (m - m_o)(2\sigma_o^2 K_{10}K_{20}) + (\sigma^2 - \sigma_o^2)(K_{10}^2 + \sigma_o^2 K_{20}^2).$$

Upon canceling terms and making the reasonable assumption that

$$\int G_{NN}(f,m_o,\sigma_o^2)\ df >> \tfrac{1}{2}\sigma_o^4 K_{20}^2 ,$$

we note that equation (B-10) reduces to

$$\sigma_u^2(m,\sigma^2) \approx \sigma^2(K_{10}^2 + \sigma_o^2 K_{20}^2) + (m - m_o)\, 2\sigma_o^2 K_{10}K_{20}$$

$$+ \int G_{NN}(f,m_o,\sigma_o^2)df. \qquad \text{(B-11)}$$

Finally, if the ATF has, in fact, achieved steady-state condition so that the only variations in σ_u^2 are those due to σ^2, e.g., if $m = mo$, then

$$\sigma_u^2(m_o,\sigma^2) \approx \sigma^2 K_{BDI}^2(mo,\sigma_o^2) + \int G_{NN}(f,m_o,\sigma_o^2)df, \qquad \text{(B-12)}$$

where

$$K_{BDI}^2(mo,\sigma_o^2) \equiv K_{10}^2 + \sigma_o^2 K_{20}^2. \qquad \text{(B-13)}$$

Since $\frac{\partial m_u}{\partial \sigma} = \sigma K_2$, an alternative expression for K_{BDI}^2 is

$$K_{BDI}^2(m_o,\sigma_o^2) = \left(\frac{\partial m_u}{\partial m}\right)^2_{m_o,\sigma_o} + \left(\frac{\partial m_u}{\partial \sigma}\right)^2_{m_o,\sigma_o}. \qquad \text{(B-14)}$$

INITIAL DISTRIBUTION LIST

Addressee	No. of Copies
COMSUBDEVGRUTWO	1
CNO, OP-02 (2), -224, -22, -942U, -953, -981G, -009T (2)	9
CNM, ASW-14 (2), -23	3
DDR&E (G. Cann)	2
NAVSHIPRANDCEN, CARD	2
NAVELECSYSCOMHQ, PME-107	2
NAVSEASYSCOMHQ, SEA-06H1, -06H2, -660, -660D, -660F (2), -660F1, -660B1, PMS-393, -396	10
DTNSRDC	2
NELC	1
NAVUSEACEN	1
NISC, Code 20, 2252 (12)	13
NAVPGSCOL	2
DDC, Alexandria	12
Naval Coastal Lab, Panama City, FL (T. Watson, Code 732)	1